Hybrid InGaP nanobeam on silicon photonics for efficient four wave mixing

Gabriel Marty, Sylvain Combrié, Alfredo de Rossi, Fabrice Raineri

Hybrid InGaP nanobeam on silicon photonics for efficient four wave mixing

Cite as: APL Photonics 4, 120801 (2019); https://doi.org/10.1063/1.5119919
Submitted: 16 July 2019 . Accepted: 13 November 2019 . Published Online: 05 December 2019

Gabriel Marty, Sylvain Combrié, Alfredo De Rossi, and Fabrice Raineri

Hybrid InGaP nanobeam on silicon photonics for efficient four wave mixing

Cite as: APL Photon. 4, 120801 (2019); doi: 10.1063/1.5119919
Submitted: 16 July 2019 • Accepted: 13 November 2019 •
Published Online: 5 December 2019

Gabriel Marty,[1,2] Sylvain Combrié,[2] Alfredo De Rossi,[2] and Fabrice Raineri[1,3,a)]

AFFILIATIONS

[1]Centre de Nanosciences et de Nanotechnologies (C2N), CNRS, Univ. Paris Sud, Univ. Paris Saclay, F-91120 Palaiseau, France
[2]Thales Research and Technology France, 1 avenue Augustin Fresnel, F-91120 Palaiseau, France
[3]Université de Paris, Centre de Nanosciences et de Nanotechnologies (C2N), F-91120 Palaiseau, France

Note: This article is part of the Special Topic on Hybrid Integration beyond Silicon Photonics.
[a)]**Electronic mail:** fabrice.raineri@c2n.upsaclay.fr

ABSTRACT

We report the design, fabrication, and characterization of a photonic crystal microresonator exhibiting a constant free spectral range. More than 50 resonances with $Q > 2 \times 10^5$ are observed in a 200 μm long and 650 nm wide III–V semiconductor cavity heterogeneously integrated on a silicon photonic circuit (Silicon on Insulator). We measured stimulated four wave mixing with a −12 dB signal to idler conversion. Two photon absorption is prevented owing to the wide electronic bandgap of the III–V semiconductor (indium gallium phosphide) enabling the possibility to use sufficiently large optical power densities for efficient nonlinear parametric interactions.

I. INTRODUCTION

The need for optical interconnects is currently driving huge efforts in the development of photonic devices integrated on-chip.[1] Like their electronic counterparts, these devices are required to be energy efficient, robust, and compact. On-chip, nonlinear processes are particularly interesting for ultrafast signal processing[2] or quantum light generation.[3] The efficiency of these processes depends on the ability to confine light in the smallest volume with the longest interaction length altogether with the smallest losses. Silicon may be an attractive material for nonlinear integrated optics at first glance because of its high nonlinearity, high refractive index, and low propagation losses. However, two photon absorption (TPA) is a major limitation when the targeted nonlinear process occurs in the telecom windows, as the photon energy is greater than half of the material bandgap energy.[4] To circumvent this limitation, the use of hybrid structures, where a material with a bandgap wide enough to cancel TPA (such as III–V semiconductor alloys) is heterogeneously integrated on silicon, is an excellent solution. Indeed, these structures benefit from the advantages of a silicon circuitry in the linear regime and add new nonlinear functionalities in a similar way that allows us to add direct bandgap material to fabricate integrated lasers.[5]

One of the reasons why optical fibers are so effective in nonlinear optics[6] is that the essential requirement of phase matching (momentum conservation, $2k_p = k_i + k_s$) is easily fulfilled in four wave mixing (FWM) processes as it only requires a nearly flattened dispersion over the spectral range of interest. In this work, we focus our attention on FWM in Photonic Crystal (PhC) cavities. In resonators, in contrast to waveguides, the phase matching condition is reformulated in terms of selection rules for the interacting modes. More critical is to fulfill the energy conservation ($2\omega_p = \omega_s + \omega_i$). Resonant four wave mixing has been extensively studied in integrated microrings where energy conservation is ensured by tailoring the dispersion of their constituting waveguide. The strength of the parametric interaction scales inversely with the radius of the resonator,[7] which has a minimum value set by the maximum acceptable bending losses. On the other hand, photonic crystal cavities provide very strong light matter interaction, thanks to the provided confinement of light in diffraction limited volume. Outstanding results were obtained for several optical functionalities ranging from electrically pumped lasers,[8] all-optical switching,[9] or optomechanics.[10]

However, satisfying the energy and phase matching conditions is not trivial in PhC cavities and dispersion engineering is required. The resonance frequencies have to be precisely controlled. Several approaches have been proposed to achieve FWM, such as the use of PhC coupled 1D[11] or 2D[12] cavities, but to our knowledge with limited power efficiency. The fundamental issue remains the alignment of three resonances which becomes increasingly challenging as the resonance linewidth decreases. A proposal for the individual frequency optimization method with relatively low Q-factors was made,[13] but the related experiment has not yet been performed. Here, we demonstrate experimentally a PhC resonator integrated on a silicon photonic platform with about 50 resonances forming a comb with constant FSR (Free Spectral Range), thus matching the requirements for parametric interaction.

II. CONCEPT

Our nanobeam cavity consists in a ridge waveguide drilled with circular holes where the hole to hole distance, a, is varied in order to build high reflectivity mirrors [see Fig. 1(a)]. In this case, the electromagnetic (EM) field decay in the mirrors is not simply exponential as in a perfectly periodic structure but depends directly on the evolution of the lattice constant a in the longitudinal direction. Thus, the EM field in the cavity writes $E \propto e^{-A(x)x}$, where $A(x)$ is the spatially dependent field decay at the position x. As in the work of Bazin *et al.*,[14] we calculate the dependence of A with a and retrieve the evolution of a with x in order to shape the first order resonant mode E-field envelope into a Gaussian. This envelope is characterized by its full width at half maximum (FWHM) which can be adjusted at will by changing $a(x)$. An example of the calculated dependence of a with x is plotted in Fig. 1(b). This is for a 650 nm wide, 290 nm thick nanobeam cavity made in a semiconductor slab (n = 3.13) encapsulated in SiO_2 where the hole radius r = 110 nm and FWHM = 4 μm. As can be seen, a increases from 340 nm in the center of the cavity (A = 0 at 1550 nm) to 382 nm at its extremities (maximum of A which corresponds to the middle of the photonic bandgap at 1550 nm). 10 holes are added on the sides of the cavity with a = 382 nm to avoid leakage of the EM field in the longitudinal direction. Such a design allows us to obtain in simulation [3D finite-difference time domain (FDTD)] a Gaussian shaped mode at 193.103 THz (1552.5 nm) with a Q factor beyond 10^7. This high Q value is expected: this mode exhibits a reduced amplitude of the E-field distribution at spatial frequencies inside the light cone which thereby diminishes radiative losses,[15] while keeping the modal volume close to the diffraction limit. Higher order modes are allowed. Their spatial distribution in energy and their resonant frequency are given in Figs. 1(c) and 1(d) together with those of the fundamental modes. The modes are equally spaced in frequency, separated by a FSR of 1.4 THz (11 nm in wavelength). The Q factor of these modes is all above 10^7. The spatial envelope of the modes contains a number of lobes equals to their order, and as can be seen in Fig. 1(c), it can be accurately fitted by a (p-1)th order Hermite-Gauss function with p being the order or the mode (0th order corresponding to a Gaussian function). Thus, the eigenmodes of our nanobeam cavity map onto those of a quantum mechanics harmonic oscillator. From this, we can infer that the design remarkably results in a parabolic effective photonic potential for the photons [plotted in Fig. 1(d)], built under the only condition of achieving a spatially gaussian fundamental mode and not a parabolic evolution of the lattice constant a. An effective potential with approximated Hermite-Gauss modes has already been observed in two-dimensional photonic crystals cavities,[16] implementing an effective bichromatic photonic lattice[17] which is described by the André-Aubry potential. Others demonstrations of this concept have also been proposed with the direct modulation of the width of the membrane in PhC[18] or in fibers.[19] A striking feature of this PhC multimode cavity design is its flexibility. Particularly, the FSR can be adjusted to a large extent as shown in Fig. 2(a), the FSR being related to the FWHM of the fundamental Gaussian mode, which is our key design parameter. We note a parabolic dependence of the FSR with $(\text{FWHM})^{-1}$, while in

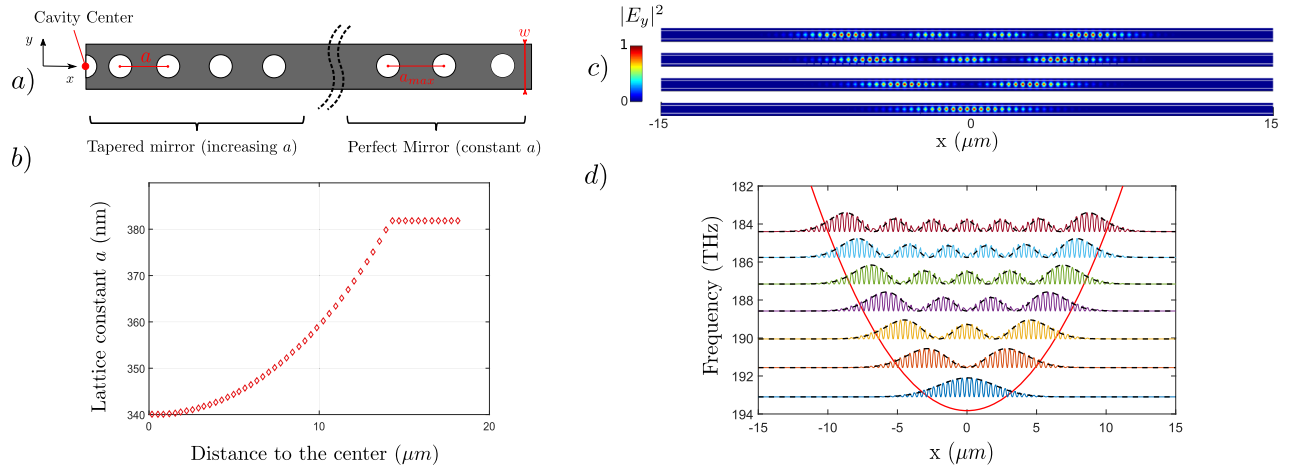

FIG. 1. (a) Schematic of the nanobeam cavity with a tapered mirror and a perfect periodic mirror. (b) Evolution of the distance between the holes. (c) Maps of the electric field amplitude $|E_y|^2$ of the first four modes in the Z = 0 plane. (d) Calculated first seven eigenmodes represented along the x-axis, Hermite-Gauss enveloped (dashed), and the corresponding parabolic potential. Note that the frequency points downward.

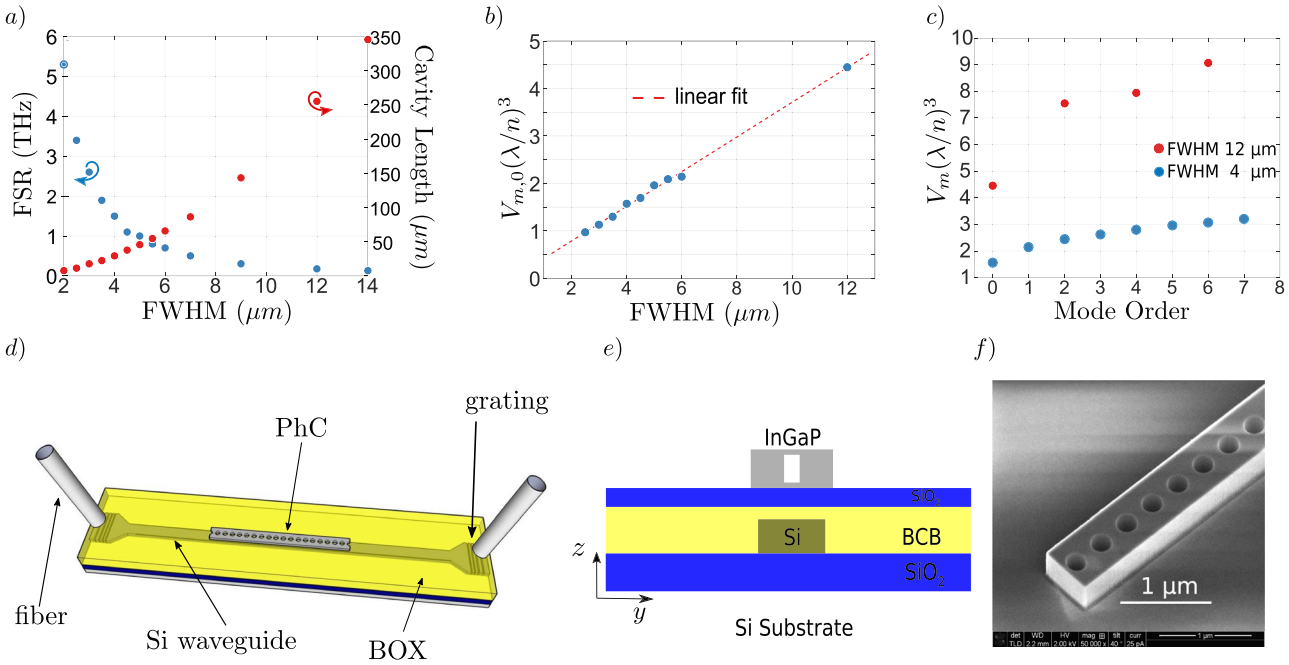

FIG. 2. (a) Evolution of the FSR with the FWHM of the fundamental mode and the corresponding length of the cavity. (b) Evolution of the volume of the fundamental mode with respect to the FWHM. The red dotted line is a linear fit. Volume units are normalized with the diffraction volume. (c) Mode volume of the first modes of a 4 μm and a 12 μm FWHM cavity. (d) 3D and (e) YZ cut schematics of the layers of the integrated structure. (f) SEM picture of an InGaP nanobeam after ICP etching.

a Fabry-Perot or a ring resonator, the FSR is linearly dependent with the inverse of the length of the cavity. The frequency of the fundamental mode also slightly changes from 192.5 THz (1557.4 nm) to 193.8 THz (1546.7 nm) when the FSR decreases from 2.4 THz (19 nm) to 130 GHz (1 nm) for identical geometric parameters (dimension of the ridge, hole diameter, and initial and final hole period). Moreover, as FWHM increases, the full cavity length strongly increases due to our design rules previously described. The calculated mode volume[20] of the first order mode, $V_{m,0}$, [see Fig. 2(b)] grows linearly with the FWHM, ranging from 0.76 to 4.45 $\left(\frac{\lambda}{n}\right)^3$ when the FWHM increases from 2 μm to 12 μm. Figure 2(c) shows the calculated volume of the higher order modes for FWHM = 4 μm and FWHM = 12 μm. As expected, it increases with the mode order, the largest change being observed going from the fundamental to 2nd order mode. $V_{m,p}$ doubles its value only when p = 6.

III. RESULTS

Schematics of the hybrid structure are represented in Figs. 2(d) and 2(e). As indicated, our nanobeam cavities are fabricated in Indium Gallium Phosphide (InGaP) slabs transferred onto a Silicon on Insulator (SOI) waveguide circuitry. InGaP is an interesting III–V semiconductor for nonlinear photonics. With silicon, it shares a large refractive index (3.13) at telecom wavelength and a large nonlinearity, $n_2 = 0.6 \times 10^{-17}$ m^2/W.[21,22] In addition, its large bandgap (Eg ≈ 2 eV) is superior to the energy of two photons at telecom wavelength (1.6 eV), therefore mitigating nonlinear absorption.[23] benzocyclobutene adhesive bonding is used to integrate InGaP onto SOI.[24] The nanobeam cavity is fabricated on top of a waveguide using negative single pass e-beam lithography with hydrogen silsesquioxane resist at a writing resolution of 0.5 nm. Holes are drilled with Inductive Coupling Plasma (ICP) etching using HBr/He/O2 gas mix. As can be seen on the SEM picture of Fig. 2(f), very smooth sidewalls are obtained from the optimized etching process. As previously demonstrated, the coupling between the silicon waveguide and the nanobeam can be tuned by changing the thickness of the adhesive silica layer or the width of the feeding waveguide.[25] The linear transmission of the fabricated structures is characterized using an optical coherent tomography (OCT) setup,[16] employing a spectrally narrow swept laser source which is coupled to SOI waveguides through grating couplers. The transmission spectra display a comb of high Q resonances, as can be seen in Fig. 3(a). The insertion losses of the couplers are estimated by measuring the transmitted power off resonance. It reaches a quite significant value of −17 dB due to the unoptimized design and fabrication. This could be further improved as couplers with coupling efficiency below −1 dB were recently demonstrated.[26] 54 resonances can be counted in Fig. 3(a), and this number being limited, here, by the transmission bandwidth of the gratings couplers. This spectrum corresponds to the transmission of a cavity with FWHM = 12 μm. The high reflectivity bandwidth of the mirrors of the cavity, which is determined by the width of the photonic bandgap of the PhC (~40 THz), allows the existence of this high number of resonances. The mode order of each resonance is plotted in Fig. 3(b) as a function of its frequency. The linearity of the obtained curve is, at first glance, a proof that the FSR is constant as the mode order

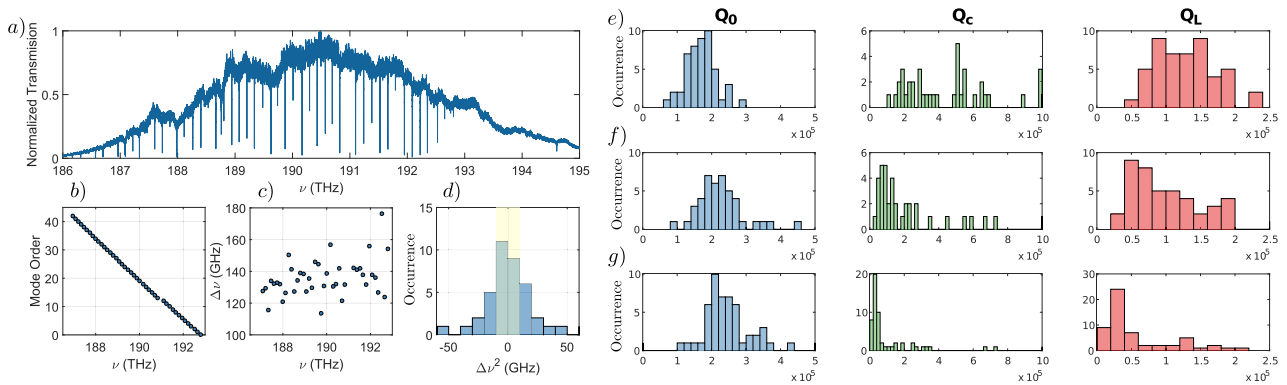

FIG. 3. (a) Normalized raw transmission spectrum of the full device (including grating couplers), (b) extracted eigenfrequencies, (c) FSR vs frequency, and (d) histogram of the frequency mismatch $\Delta^2\nu$ of three consecutive resonances. Statistical analysis of the values of *Q* factors of a nanobeam with 12 μm FWHM fed with a waveguide width of (e) 400 nm (undercoupled regime), (f) 550 nm (critically coupled regime), and (g) 500 nm (overcoupled regime).

increases. Only one resonance was not detected in this measurement. Looking closely at the FSR as a function of the frequency [Fig. 3(c)], we can see that it oscillates in a 100 GHz range and stabilizes toward a constant value around 130 GHz. We infer that this oscillation is due to a Moiré effect that happens during the discretization of the e-beam writing grid. A histogram of the second order dispersion for three consecutive resonances is plotted in Fig. 3(d). This is the important parameter for FWM that needs to be close to 0 for perfectly matched resonances. The region highlighted in yellow shows the triplets with a frequency mismatch inferior to 10 GHz. The distribution appears to be normal and centered around 0. The linewidth of the resonances [~2 GHz for Q = 100 000 at 193.415 THz (1550 nm)] defines a phase matching bandwidth, i.e., the maximum frequency mismatch allowed to keep all 3 interacting waves resonant. For example, 3 resonances with Q = 100 000 can support a maximal mismatch of 6 GHz before one of the waves involved in FWM is out of resonance. A coupled mode theory model related to the measurement technique is used to deduce the intrinsic (without waveguide) and coupling (induced by the coupling to the waveguide) losses of all resonant modes. Figures 3(e)–3(g) show the dependence of the quality factors Q_0 (linked to intrinsic loss), Q_c (coupling loss), and Q_L (total loss) factors on the width of the feeding SOI waveguide. The statistics of Q_0 is independent of the coupling strength, as expected, and reveals that the most frequent value is around 200 000 with a maximum at 445 000, which is a record in the InGaP bonded structure. It is limited by the roughness of the etched sidewalls and the absorption of the InGaP and the silica intermediate layers. We suspect the latter to be the main limitation, and further investigations on the composition of this layer will be conducted in a near future. Q_c is strongly dependent of the width of the SOI waveguide as can be seen in Figs. 3(e)–3(g). Three representative cases are shown: the undercoupled ($Q_0 < Q_c$) regime with 400 nm wide waveguides (e), the overcoupled one ($Q_0 > Q_c$) with 500 nm waveguides (g), and the critically coupled ($Q_0 = Q_c$) one with 550 nm waveguides (f). The averaged Q_c are 440 000, 100 000, and 197 000 for 400, 500, and 550 nm wide waveguides, respectively, and the average Q_0 are 171 000 (e), 224 000 (f), and 243 000 (g). The average loaded Q, Q_L, can then be tuned from 58 000 (g) to 128 000 (e) just by changing Q_c through a change of waveguide width and reaches Q_L = 99 000 at critical coupling (f). In the transmission window of the gratings, we did not observe a dispersive coupling, but some resonances can be unexpectedly undercoupled or overcoupled, which is attributed to localized default arising from fabrication.

IV. NONLINEAR EXPERIMENT

The nonlinear measurements are performed using a cavity with a FWHM of 5 μm (a total length of 60 μm). The interacting modes have a loaded Q factor of 97 000, 35 000, and 76 000, respectively, for the idler, pump, and signal modes. It corresponds to an average Q, Q_{avg} = 55 000. The pump has a lower Q factor because it is overcoupled to the waveguide, whereas the idler and pump are closer to the critical coupling. As shown in Fig. 4(a), two continuous waves (CW) tunable laser sources are used to provide the pump and signal. They are combined with a 90/10 coupler and amplified by an erbium doped fiber amplifier (EDFA). The insertion losses of this waveguide are estimated off resonance to be about −12.5 dB per grating coupler. At the output of the waveguide, we use an optical spectrum analyzer to record the output spectrum. We set the pump at resonance and scan the signal frequency. As seen in Fig. 4(b), when the signal is off-resonance, no idler peak is observed, disqualifying nonlinear generation in the Si waveguide. When the signal is tuned closer to resonance, we observe a dip in its transmitted power as expected. Simultaneously, an idler sideband is generated and reaches a maximum 13 dB above the noise floor when the signal is at resonance [see Fig. 4(c)]. From this observation, we can conclude that resonant wavelength conversion occurs in our nanobeam. The nonlinear efficiency is estimated by taking the ratio of the maximum idler power over the transmitted signal power off resonance. However, because the cavity is symmetric with respect to the Si waveguide, the emission of the generated idler is supposed to be the same in the two direction of the waveguide. Thus, we must add 3 dB to the maximum idler power, which brings the total maximum on-chip efficiency up to −12 dB for an estimated 3.16 mW pump power coupled in the SOI waveguide. Let us note that frequency conversion experiments are usually studied as a function of the pump power and should

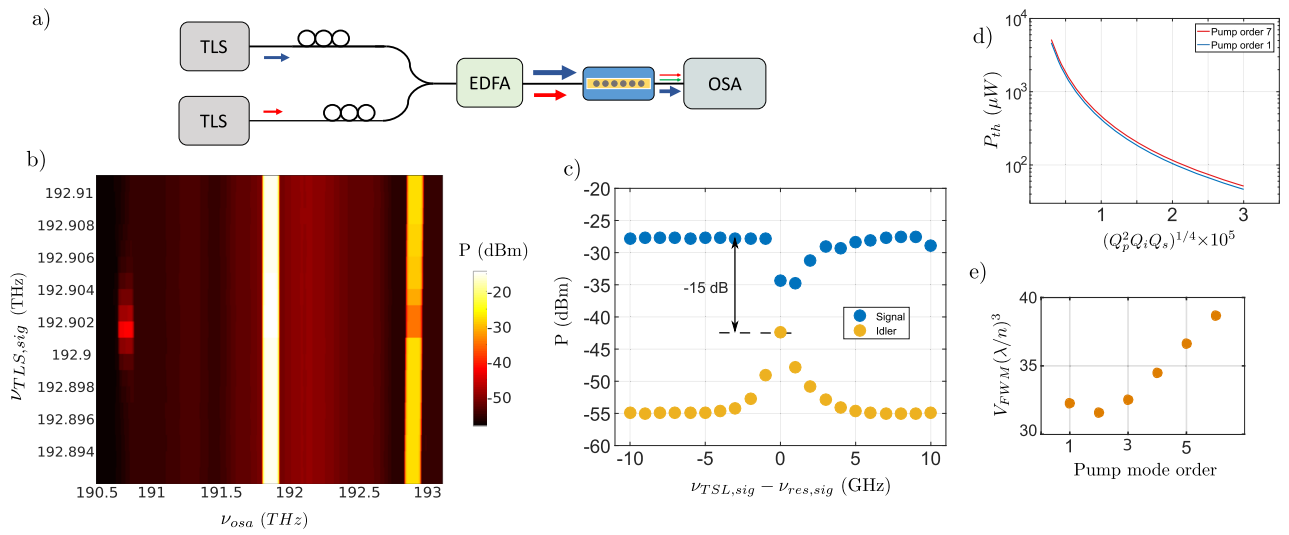

FIG. 4. (a) Experimental setup for nonlinear conversion measurements: TLS = Tunable Laser Source, EDFA = Erbium Doped Fiber Amplifier, and OSA = Optical Spectrum Analyzer. (b) Map of the power intensity recorded for a fixed pump and a signal frequency $\nu_{TSL,sig}$ sweeping from 192.910 THz to 192.892 THz. (c) Extracted signal and idler power as a function of the position of the signal frequency $\nu_{TSL,sig}$ relatively to its resonance $\nu_{res,sig}$. (d) Theoretical parametric threshold of the nanobeam cavity as a function of the geometric average *Q*. The blue curve is when mode 1 is pumped, and the red curve is when it is mode 7. (e) Normalized interacting volume as a function of the geometric average *Q* calculated with 3D FDTD.

show a quadratic dependence for FWM (under oscillation threshold). In our particular platform, such a study is complicated by the thermal effects induced by the pump. In fact, it has been shown that the coupled pump level strongly affects the dispersion of the resonant modes of the cavity[27] which results in a nontrivial scaling of the nonlinear efficiency with the pump level.

In order to consolidate our demonstration of resonant FWM inside the nanobeam cavity, we compare our experimental results with the theoretical predictions. To do so, we use a time dependant coupled-mode theory (CMT) to describe our system.[13] For an undepleted degenerate pump, the evolution of the complex envelope of the different fields is described by

$$\frac{\partial a_p}{\partial t} = (-i2\pi\delta\nu_p - \frac{\Gamma_p}{2} - \kappa_p)a_p + i\sqrt{\kappa_p}s_p^+,$$
$$\frac{\partial a_s}{\partial t} = (-i2\pi\delta\nu_s - \frac{\Gamma_s}{2} - \kappa_s)a_s + i\sqrt{\kappa_s}s_s^+ - 2\gamma_{FWM}a_p^2 a_i^*,$$
$$\frac{\partial a_i}{\partial t} = (-i2\pi\delta\nu_i - \frac{\Gamma_i}{2} - \kappa_i)a_i - 2\gamma_{FWM}a_p^2 a_s^*,$$

where the subscript p, s, and i refers to the pump, signal, and idler wave, respectively. Γ is the total loss rate, composed of $\Gamma = \Gamma_0 + 2\kappa$, where Γ_0 and κ are, respectively, the intrinsic and coupling losses. The factor 2 for the coupling accounts for the symmetric emission of the nanobeam inside the waveguide. They are related to Q by the relation $Q_L = \frac{2\pi\nu}{\Gamma}$, $Q_0 = \frac{2\pi\nu}{\Gamma_0}$, and $Q_c = \frac{\pi\nu}{\kappa}$. $\delta\nu$ is the difference between the parametric frequency and the resonance frequency, which is shifted by thermal, self-phase, and cross-phase modulation effects, and s^+ is the incoming laser fields. $|a|^2$ represents the intracavity energy of one mode. γ_{FWM} is the FWM coupling coefficient,

$$\gamma_{FWM} = \frac{c_0 n_2 2\pi\nu_p}{\varepsilon_r V_{FWM}},$$

where c_0 is the speed of light, n_2 is the nonlinear index, ν_p is the pump frequency, ε_r is the permittivity, and V_{FWM} is the nonlinear volume. V_{FWM} is the parameter characterizing the strength of the nonlinear interaction, by taking into account the spatial overlap of the different waves in the cavity. It writes[16]

$$V_{FWM,p,s,i}^{-1} = \frac{\varepsilon_0^2\varepsilon_r^2}{4}\int_V \zeta \frac{2(\mathbf{e}_p^*\cdot\mathbf{e}_i)(\mathbf{e}_p^*\cdot\mathbf{e}_s) + (\mathbf{e}_p^*\cdot\mathbf{e}_p^*)(\mathbf{e}_s\cdot\mathbf{e}_i)}{3}dV.$$

Here, $\mathbf{e_p}$, $\mathbf{e_s}$, and $\mathbf{e_i}$ represent, respectively, the normalized pump, signal, and idler cavity modes. The filling factor ζ equals 1 when the fields are in the nonlinear medium and 0 otherwise. We define the outgoing fields as s^-. In the limit of low parametric gain and when all the fields are resonant ($\delta\nu = 0$), the nonlinear efficiency is defined as

$$\eta_{FWM} = \frac{|s_i^-|^2}{|s_s^+|^2} = |\gamma_{FWM}|^2.$$

By taking into account the nonlinear volume of the cavity, $V_{FWM} = 40\left(\frac{\lambda}{n}\right)^3$, the maximum theoretical efficiency for the injected pump is calculated to be ηth = −3 dB. The discrepancy is about one order of magnitude in comparison to the measured value. We attribute this difference to the nonlinear response of the cavity at the pump wavelength inducing a frequency shift of the resonance, diminishing thereby the coupled intracavity intensity. A detailed study of the nonlinear interaction inside the nanobeam is beyond the scope of this paper, but we clearly see that there is room for further development, particularly about the dynamic of the interaction between the modes.

To push further the analysis, we address the perspective of parametric oscillation with this type of cavities. In the case where the

TABLE I. Comparison of continuous wave FWM nonlinear efficiency conversion in PhC cavities. (CROW: Coupled Resonators Optical Waveguide).

Geometry	Material	Q_{avg}	On chip power (μW)	η_{NL} (dB)	Reference
1D PhC (3 coupled cavities)	Si	4000	60	−55	11
2D PhC CROW	Si	600 000	100	−35	12
2D PhC CROW	InGaP	70 000	36	−24	28
1D PhC (single cavity)	InGaP	55 000	3160	−14	*This work*

TABLE II. Comparison of continuous wave FWM nonlinear efficiency conversion in integrated devices. (CROW: Coupled Resonators Optical Waveguide).

Geometry	Material	Q_{avg}	On chip power (μW)	η_{NL}(dB)	Footprint (μm^2)	Reference
Ring	Hydrex	10^6	6160	−26	5730	31
Ring	Si—graphene	9000	8000	−37	314	32
Ring-CROW	Si	x	100 000	−21	4140	33
Ring	AlGaAsOI	44 000	7000	−12	929	30
PhC on SOI	InGaP	55 000	3160	−12	39	*This work*

pump, signal, and idler frequencies are resonant and modes are overcoupled, the power level for the threshold of parametric oscillation is formulated for PhC cavities in terms of the nonlinear interacting volume,[16]

$$P_{th} \approx \frac{\pi \varepsilon_r v_p V_{FWM}}{2 c_0 n_2 Q_{avg}^2},$$

where v_p is the pump frequency, n_2 is the nonlinear index, $Q_{avg} = (Q_p^2 Q_i Q_s)^{\frac{1}{4}}$ is the geometrical average of the loaded Q. Figure 4(d) shows the evolution of the threshold as a function of Q_{avg}, with P_{th} = 5 mW for $Q_{avg} \approx 50\,000$ and P_{th} = 50 μW for $Q_{avg} \approx 500\,000$. Considering the range of Q factors achieved in our system, submilliwatt threshold is already reachable (0.4 mW with Q = 10^5, pump in mode (1). An interesting feature is that, as can be seen in the same figure, P_{th} weakly increases by choosing to pump the system in a higher order mode. This can be explained by the moderate increase in V_{FWM} with the mode order [see Fig. 4(e)], which is an interesting characteristic of our nanobeam cavities.

V. COMPARISON WITH OTHER MICRORESONATORS AND CONCLUSION

We have demonstrated the fabrication of a photonic crystal resonator exhibiting a large number of high-Q eigenmodes which are spaced evenly to form a comb of resonances. This resonator is made of InGaP which has a large electronic bandgap, which effectively suppresses two-photon absorption in the telecom spectral range. The compact nanobeam resonators are heterogeneously integrated to a silicon photonic circuit. A statistical analysis reveals a most probable intrinsic Q factor about 2×10^5. We have showed that these cavities are very interesting for efficient FWM by reporting a frequency conversion in a single integrated nanobeam cavity of −12 dB.

In order to compare our results to previous investigations on FWM in microresonators, we present two tables. Table I deals with demonstrations of FWM in the continuous regime with PhC cavities. The table reports the characteristics of the systems and the obtained efficiencies. As can be seen, to the best of our knowledge, our results constitute a record in terms of absolute conversion efficiency, with a 10 dB improvement to a previously reported result.[28] Such a high value is linked to the combination in our platform of advantageous physical properties such as the use of a TPA-free highly nonlinear material and a high Q factor. Very importantly, our hybrid system also allows excellent insertion and collection of light in and out of the cavity as well as improved heat sinking compared to air bridged PhCs.[29] For these reasons, we are able to insert higher power levels in our cavities, inducing a higher conversion efficiency. Indeed, in the other systems, the input power giving the maximum efficiency is limited by TPA in Si-based structures and/or by heat sinking in air-bridged ones. The performance of our device is reported in Table II together with that of ring resonators. Our hybrid nanobeam cavity is comparable in terms of conversion efficiency with the state of the art ring-based system, i.e., rings made in a thin AlGaAs layer bonded on SiO2/Si,[30] but our result is obtained for a weaker pump power within a footprint which is 30 times smaller. It is a clear demonstration that PhC cavities can allow a larger conversion efficiency than in ring resonators for the same Q and input power due to their ability to confine light in a smaller volume. We believe that this work contributes to showing that nanophotonic devices are coming of age and constitute a unique way of providing chip-scale integrated, compact, and energy efficient photonic components.

ACKNOWLEDGMENTS

This work was supported by a public grant overseen by the French National Agency (ANR) as part of the "Investissements d'Avenir" program (Labex NanoSaclay reference Grant No. ANR-10-LABX-0035). This work has also received funding from the European Research Council (ERC) under the Horizon 2020 research and

innovation programme (HYPNOTIC PROJECT Grant Agreement No. 726420).

REFERENCES

[1]M. J. Kobrinsky, B. A. Block, J.-F. Zheng, B. C. Barnett, E. Mohammed, M. Reshotko, F. Robertson, L. Scott, I. Young, and K. Cadien, "On-chip optical interconnects," Intel Technol. J. **8**(2), 129–141 (2004).

[2]H. Hu, F. Da Ros, M. Pu, F. Ye, I. Kasper, E. P. da Silva, M. Nooruzzaman, Y. Amma, Y. Sasaki, T. Mizuno *et al.*, "Single-source chip-based frequency comb enabling extreme parallel data transmission," Nat. Photonics **12**(8), 469 (2018).

[3]L. Caspani, C. Xiong, B. J. Eggleton, D. Bajoni, M. Liscidini, M. Galli, R. Morandotti, and D. J. Moss, "Integrated sources of photon quantum states based on nonlinear optics," Light: Sci. Appl. **6**, e17100 (2017).

[4]Y. Liu and H. K. Tsang, "Time dependent density of free carriers generated by two photon absorption in silicon waveguides," Appl. Phys. Lett. **90**(21), 211105 (2007).

[5]R. Gunther, A. Amin, P. Cardile, U. Dave, A. De Groote, Y. De Koninck, S. Dhoore, X. Fu, A. Gassenq, N. Hattasan *et al.*, "III-V-on-silicon photonic devices for optical communication and sensing," Photonics **2**(3), 969–1004 (2015).

[6]G. P. Agrawal, "Nonlinear fiber optics," in *Nonlinear Science at the Dawn of the 21st Century* (Springer, 2000), pp. 195–211.

[7]L. G. Helt, M. Liscidini, and J. E. Sipe, "How does it scale? Comparing quantum and classical nonlinear optical processes in integrated devices," J. Opt. Soc. Am. B **29**(8), 2199–2212 (2012).

[8]G. Crosnier, D. Sanchez, S. Bouchoule, M. Paul, G. Beaudoin, I. Sagnes, R. Raj, and F. Raineri, "Hybrid indium phosphide-on-silicon nanolaser diode," Nat. Photonics **11**(5), 297 (2017).

[9]C. Husko, A. De Rossi, S. Combrié, Q. V. Tran, F. Raineri, and C. W. Wong, "Ultrafast all-optical modulation in GaAs photonic crystal cavities," Appl. Phys. Lett. **94**(2), 021111 (2009).

[10]E. Gavartin, R. Braive, I. Sagnes, O. Arcizet, A. Beveratos, T. J. Kippenberg, and I. Robert-Philip, "Optomechanical coupling in a two-dimensional photonic crystal defect cavity," Phys. Rev. Lett. **106**, 203902 (2011).

[11]S. Azzini, D. Grassani, M. Galli, D. Gerace, M. Patrini, M. Liscidini, P. Velha, and D. Bajoni, "Stimulated and spontaneous four-wave mixing in silicon-on-insulator coupled photonic wire nano-cavities," Appl. Phys. Lett. **103**(3), 031117 (2013).

[12]N. Matsuda, T. Kato, K.-i. Harada, H. Takesue, E. Kuramochi, H. Taniyama, and M. Notomi, "Slow light enhanced optical nonlinearity in a silicon photonic crystal coupled-resonator optical waveguide," Opt. Express **19**(21), 19861–19874 (2011).

[13]Z. Lin, T. Alcorn, M. Loncar, S. G. Johnson, and A. W. Rodriguez, "High-efficiency degenerate four-wave mixing in triply resonant nanobeam cavities," Phys. Rev. A **89**, 053839 (2014).

[14]A. Bazin, R. Raj, and F. Raineri, "Design of silica encapsulated high-Q photonic crystal nanobeam cavity," J. Lightwave Technol. **32**(5), 952–958 (2014).

[15]Y. Akahane, T. Asano, B.-S. Song, and S. Noda, "High-Q photonic nanocavity in a two-dimensional photonic crystal," Nature **425**(6961), 944 (2003).

[16]S. Combrié, G. Lehoucq, G. Moille, A. Martin, and A. De Rossi, "Comb of high-Q resonances in a compact photonic cavity," Laser Photonics Rev. **11**(6), 1700099 (2017).

[17]F. Alpeggiani, L. C. Andreani, and D. Gerace, "Effective bichromatic potential for ultra-high Q-factor photonic crystal slab cavities," Appl. Phys. Lett. **107**(26), 261110 (2015).

[18]M. C. F. Dobbelaar, S. Greveling, and D. van Oosten, "Large area photonic crystal cavities: A local density approach," Opt. Express **23**(6), 7481 (2015).

[19]M. Sumetsky, "Microscopic optical buffering in a harmonic potential," Sci. Rep. **5**, 18569 (2015).

[20]The mode volume here refers to the standard cavity QED definition: $V_m = \frac{\int_V \varepsilon(r)|E(r)|^2 d^3r}{max[\varepsilon(r)|E(r)|^2]}$.

[21]C. Husko, S. Combrié, Q. V. Tran, F. Raineri, C. W. Wong, and A. De Rossi, "Non-trivial scaling of self-phase modulation and three-photon absorption in III-V photonic crystal waveguides," Opt. Express **17**(25), 22442 (2009).

[22]A. Martin, D. Sanchez, S. Combrié, A. de Rossi, and F. Raineri, "GaInP on oxide nonlinear photonic crystal technology," Opt. Lett. **42**(3), 599–602 (2017).

[23]S. Combrié, Q. V. Tran, A. De Rossi, C. Husko, and P. Colman, "High quality GaInP nonlinear photonic crystals with minimized nonlinear absorption," Appl. Phys. Lett. **95**(22), 221108 (2009).

[24]G. Crosnier, D. Sanchez, A. Bazin, M. Paul, S. Bouchoule, R. Braive, G. Beaudoin, I. Sagnes, R. Raj, and F. Raineri, "High Q factor InP photonic crystal nanobeam cavities on silicon wire waveguides," Opt. Lett. **41**(3), 579–582 (2016).

[25]Y. Halioua, A. Bazin, P. Monnier, T. J. Karle, G. Roelkens, I. Sagnes, R. Raj, and F. Raineri, "Hybrid III-V semiconductor/silicon nanolaser," Opt. Express **19**(10), 9221–9231 (2011).

[26]R. Marchetti, C. Lacava, K. Ali, X. Chen, I. Cristiani, D. J. Richardson, G. T. Reed, P. Petropoulos, and P. Minzioni, "High-efficiency grating-couplers: Demonstration of a new design strategy," Sci. Rep. **7**(1), 16670 (2017).

[27]G. Marty, S. Combrié, F. Raineri, and A. De Rossi, "efficient photonic crystal parametric source harnessing high-Q resonances," preprint arXiv:1909.08717 (2019).

[28]A. Martin, G. Moille, S. Combrié, G. Lehoucq, T. Debuisschert, J. Lian, S. Sokolov, A. P. Mosk, and A. de Rossi, "Triply-resonant continuous wave parametric source with a microwatt pump," preprint arXiv:1602.04833 (2016).

[29]A. Bazin, M. Paul, X. Lafosse, G. Beaudoin, R. Braive, I. Sagnes, R. Raj, and F. Raineri, "Thermal management in hybrid InP/silicon photonic crystal nanobeam laser," Opt. Express **22**(9), 10570–10578 (2014).

[30]M. Pu, H. Hu, L. Ottaviano, E. Semenova, D. Vukovic, L. K. Oxenløwe, and K. Yvind, "Ultra-efficient and broadband nonlinear AlGaAs-on-insulator chip for low-power optical signal processing," Laser Photonics Rev. **12**(12), 1800111 (2018).

[31]M. Ferrera, D. Duchesne, L. Razzari, M. Peccianti, R. Morandotti, P. Cheben, S. Janz, D.-X. Xu, B. E. Little, S. Chu *et al.*, "Low power four wave mixing in an integrated, micro-ring resonator with Q = 1.2 million," Opt. Express **17**(16), 14098–14103 (2009).

[32]M. Ji, H. Cai, L. Deng, Y. Huang, Q. Huang, J. Xia, Z. Li, J. Yu, and Y. Wang, "Enhanced parametric frequency conversion in a compact silicon-graphene microring resonator," Opt. Express **23**(14), 18679–18685 (2015).

[33]J. R. Ong, R. Kumar, and S. Mookherjea, "Triply resonant four-wave mixing in silicon-coupled resonator microring waveguides," Opt. Lett. **39**(19), 5653–5656 (2014).